https://doi.org/10.5194/egusphere-2026-5493
Preprint. Discussion started: 16 September 2026


# Tides of Norway: insights from a dense coastal tide gauge network

Michael G. Hart-Davis[1], Blanca E. Torunski[1], Antonio Bonaduce[2], Torbjørn Taskjelle[3], and Johnny A. Johannessen[2]

[1]Deutsches Geodätisches Forschungsinstitut, Technische Universität München (DGFI-TUM), Munich, Germany
[2]Nansen Environmental and Remote Sensing Center, Bergen, Norway
[3]Norwegian Hydrographic Service, Norwegian Mapping Authority, Stavanger, Norway

**Correspondence:** Michael G. Hart-Davis (michael.hart-davis@tum.de)

**Abstract.** Tide gauges provide highly precise observations of coastal sea-level variability, yet their spatial sparsity remains a fundamental limitation in regions characterised by complex coastal geometry. This study utilises an extensive archive of 250 short-duration tide-gauge deployments by the Norwegian Mapping Authority (Kartverket) between 2009 and 2026 to characterise tides along the Norwegian coast. We characterise the major tidal constituents and several tidal datums along the entire coastline, including the maximum tidal range and high-tide durations. Further, these data provide a unique source for global model validation, as shown by comparisons against five state-of-the-art tide models, yielding median errors of 2.4 to 3.3 cm that scale with model spatial resolution. Collectively, these results provide a high-density in situ characterisation of Norwegian tides, reveal fine-scale tidal variability that is unresolved by sparse permanent networks, and establish an observational basis for future spaceborne investigations of tidal dynamics in Norway's fjords and coastal waters.

## 1 Introduction

Few places illustrate the contrast between the predictability of astronomical forcing and the spatial complexity of its coastal expression more clearly than the Norwegian coast. Interactions among tidal energy, narrow passages, and irregular bathymetry generate interesting tidal features such as Moskstraumen off Lofoten, a series of tide-generated eddies, associated with one of the strongest flowing tidal currents in the world (Sætra et al., 2021; Lynge et al., 2010; Gjevik et al., 1997). The coastline is dotted with small islands and numerous fjords, which make studying and observing tidal dynamics both challenging and captivating.

Tide gauges are a fundamental data source for observing and understanding tidal variability and have been used to provide insights into local tidal dynamics, e.g., Cartwright et al. (1980) and Jänicke et al. (2021), whose studies also include parts of Norway. The main strength of tide gauge records is their temporal sampling, meaning relatively short records can recover significant insights into local tidal dynamics (e.g. Pugh et al., 2011; Filmer et al., 2025), with longer records aiding in recovering the full tidal signal as well as long-term variations in the tide. The general limitation of tide gauges, especially those deployed long-term, is their spatial coverage (see Hart-Davis et al., 2026a). This is particularly restrictive in regions with complex coastlines, such as the Norwegian coastline, which can lead to fine-scale variations in tidal dynamics.

The Norwegian coastline extends from the Swedish border in the Skagerrak, via the North Sea, to the Norwegian and Barents Seas and comprises a highly complex system of fjords, islands, archipelagos, and narrow passages (see Figure 1a) (Kubiak, 2019; Breili et al., 2020). The tidal field reflects both large-scale propagation through the Nordic Seas and modification by

https://doi.org/10.5194/egusphere-2026-5493
Preprint. Discussion started: 16 September 2026


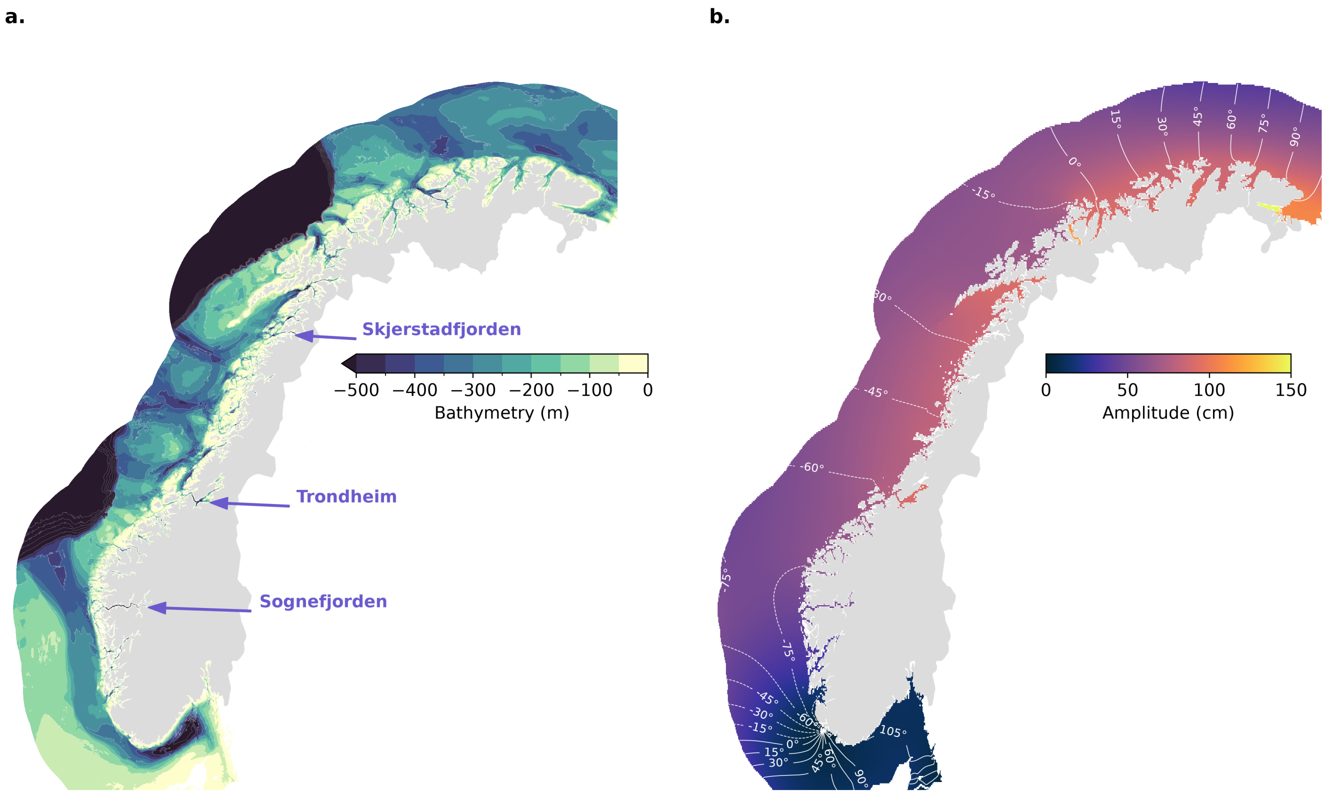


**Figure 1.** (a) Map of the bathymetry of the coast of Norway created using GEBCO22 data. (b) Map of M2 tide along the coast of Norway extracted from the EOT26 tide model. Colours represent the amplitude (cm) while the white lines demarcate the phase lags at 15-degree intervals. Several key regions are labelled for discussion in the manuscript.

regional and local bathymetry (Gjevik and Straume, 1989; Gjevik et al., 1994). Within these complex regions, tidal characteristics can vary over short distances (Hjelmervik et al., 2017), a pattern often not well captured by permanent tide gauges, primarily due to their distribution (Figure 2c).

To provide more detailed insights, this manuscript analyses a dense network of 250 tide-gauges deployed by Kartverket along the Norwegian coast (Figure 2a) between 2009 and 2026. In contrast, prior long-term records for the region were only based on 24 tide gauges (Figure 2c). This novel data source is therefore highly valuable for improving the characterisation and understanding of tidal dynamics along Norway's long, complex coastline. Moreover, it clearly strengthens the ability to evaluate the uncertainties of global tide models along the Norwegian coast. In Section 2, we introduce the data and methods, followed by a discussion of the results in Section 3, addressing tidal datums and the validation of global ocean tide models. The conclusion is provided in Section 4.

https://doi.org/10.5194/egusphere-2026-5493
Preprint. Discussion started: 16 September 2026


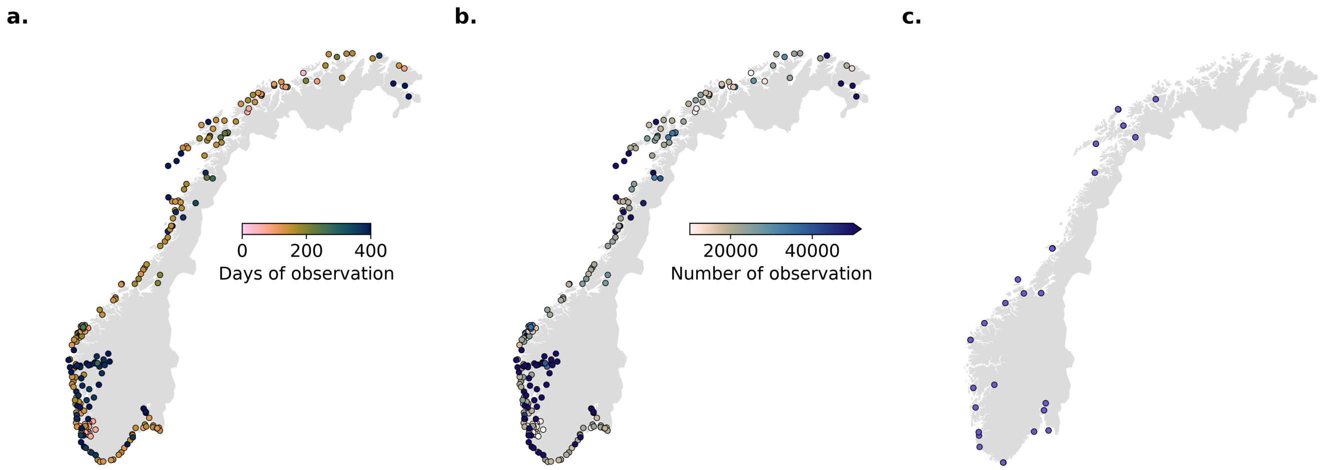


**Figure 2.** Spatial coverage of coastal tide gauge network and the associated days of observations (a) and the number of observations (b). (c) Coverage of the long-term records available in GESLA-4.

## 2 Data and Methods

The 250 tide gauges distributed along the Norwegian coast provide a substantially denser network than traditional global sea-level archives (Figure 2). Each sensor measures pressure at 1-minute intervals and is corrected for clock drift. At this stage, quality control is performed by removing outliers and errors. Water density, which is necessary to convert pressure values to sea level, is obtained from one or more Conductivity-Temperature-Depth (CTD) profiles collected during deployment, maintenance, or retrieval of the tide gauges. Once converted to sea level, the data is low-pass filtered using a Butterworth filter for dissemination at a 10-minute sampling frequency. The sampling duration of these gauges varies, with the coverage ranging from 40 days to nearly 3.5 years, with a median of 162 days, within the period 2009 to 2026.

Ideally, for tidal research, we aim to use gauges with more than 1 year of measurements to reduce contamination from nearby tidal frequencies (Piccioni et al., 2019). However, in practice, several constituents are well resolvable within the periods of these gauges. In this manuscript, we focus primarily on the eight major tidal constituents, as they are typically the largest contributors to the full tidal signal. The pairs $K_1$-$P_1$ and $S_2$-$K_2$ have Rayleigh criterion numbers that exceed the lowest sampling duration of the gauges, both at 182.62 days, which means that some energy may leak from one constituent to another in records shorter than 182.62 days between these pairs (this is the case for 60% of the records). This effect is asymmetric and has a greater impact on the smaller of the pairs, in this case, the $P_1$ and $K_2$ tides. We flag gauges where this criterion is met or not, whereby these constituents are not being further used in the tidal prediction or validation of the particular gauge.

The analysis focused on the eight principal diurnal and semidiurnal constituents $M_2$, $S_2$, $N_2$, $K_2$, $K_1$, $O_1$, $P_1$, and $Q_1$, the so-called 'major tides', which collectively represent the dominant astronomical contributions to tidal variability. In this manuscript, we derive the amplitude and phase lags for discussion and derive confidence intervals for these estimates, which we incorporate into our analysis by removing observations with uncertainties exceeding their estimates.

https://doi.org/10.5194/egusphere-2026-5493
Preprint. Discussion started: 16 September 2026


Additionally, we derive various tidal datums discussed later in this manuscript, several of which require predictions of tidal heights. To do this, we utilised Utide (Codiga, 2011) to run a harmonic analysis that extracts all tidal constituents that satisfy the Rayleigh criteria based on each particular tide gauge, from which we make a 20-year tidal height prediction. From these data, we extract the tidal datums that are discussed in the next section. It is to be emphasised, and it will be discussed later, that the length of the time series clearly influences the resulting datums. With longer records, these datums would be calculated more precisely; however, the available records still provide valuable insights into them. For the tidal analysis on the constituents and tidal heights, nodal corrections were applied throughout.

Finally, we analyse several global tide models using these tide gauges. The models selected are state-of-the-art models that utilise conventional nadir altimetry: EOT26 (Hart-Davis et al., 2021, updated), FES2022 (Lyard et al., 2021, updated), GOT5.5 (Ray, 2025), TPXO10 (Egbert and Erofeeva, 2002, updated), and DTU23 (Andersen et al., 2023). Each model is handled the same way: the individual grids are collected, and their respective amplitudes and phase lags are sampled at all 250 tide-gauge locations for the eight major tidal constituents. Bilinear interpolation is performed between the grid location and the tide-gauge location using the GMT software (Wessel et al., 2019). One final processing step was to mask out land using the same method, as some models set land to zero; bilinear interpolation would yield erroneous results in validation, particularly in regions where models lack measurements due to their spatial resolution. Once the constituents are obtained, the root-mean-square (RMS) is calculated for each of the models for each constituent, after which the root-square-sum error (RSS) is calculated for each tide gauge location for each model, with the sum referring to the sum of the individual constituents, following the methods described in Stammer et al. (2014).

## 3 Results

### 3.1 Tidal constituents

The tidal amplitudes provide a primary characterisation of the spatial variability within the Norwegian tidal field (Figure 3). Among the eight major constituents considered herein, $M_2$ appears most dominant, followed by the remaining semidiurnal and diurnal constituents at substantially smaller amplitudes. This pattern is consistent with the broader distribution of coastal tides, for which $M_2$ commonly constitutes the largest individual harmonic contribution (Hart-Davis et al., 2026a). Despite these differences in magnitude, the constituent fields exhibit a significant degree of spatial coherence.

The amplitudes are generally lowest along the southern Norwegian coastline within the Skagerrak, then increase along the western coast and remain comparatively large across much of the central and northern coasts of Norway. This geographical structure is most pronounced for the semidiurnal constituents $M_2$, $S_2$, $N_2$, and $K_2$, which show broadly coincident regions of small and large amplitude. The relatively weak tides in southern Norway are attributable to the proximity of the North Sea amphidromic system, where semidiurnal tidal amplitudes decrease significantly (seen in Figure 1b).

Further from this region, amplitude increases along the Norwegian margin. Superimposed on this northward coastal progression, the denser gauge network reveals substantial variability over much shorter spatial scales, see Figure A1 for a comparison to the long-term records from TICON-4. This is especially evident along the highly dissected western and northern coastline, where neighbouring gauges can record significant amplitude differences despite close geographical proximity.

https://doi.org/10.5194/egusphere-2026-5493
Preprint. Discussion started: 16 September 2026


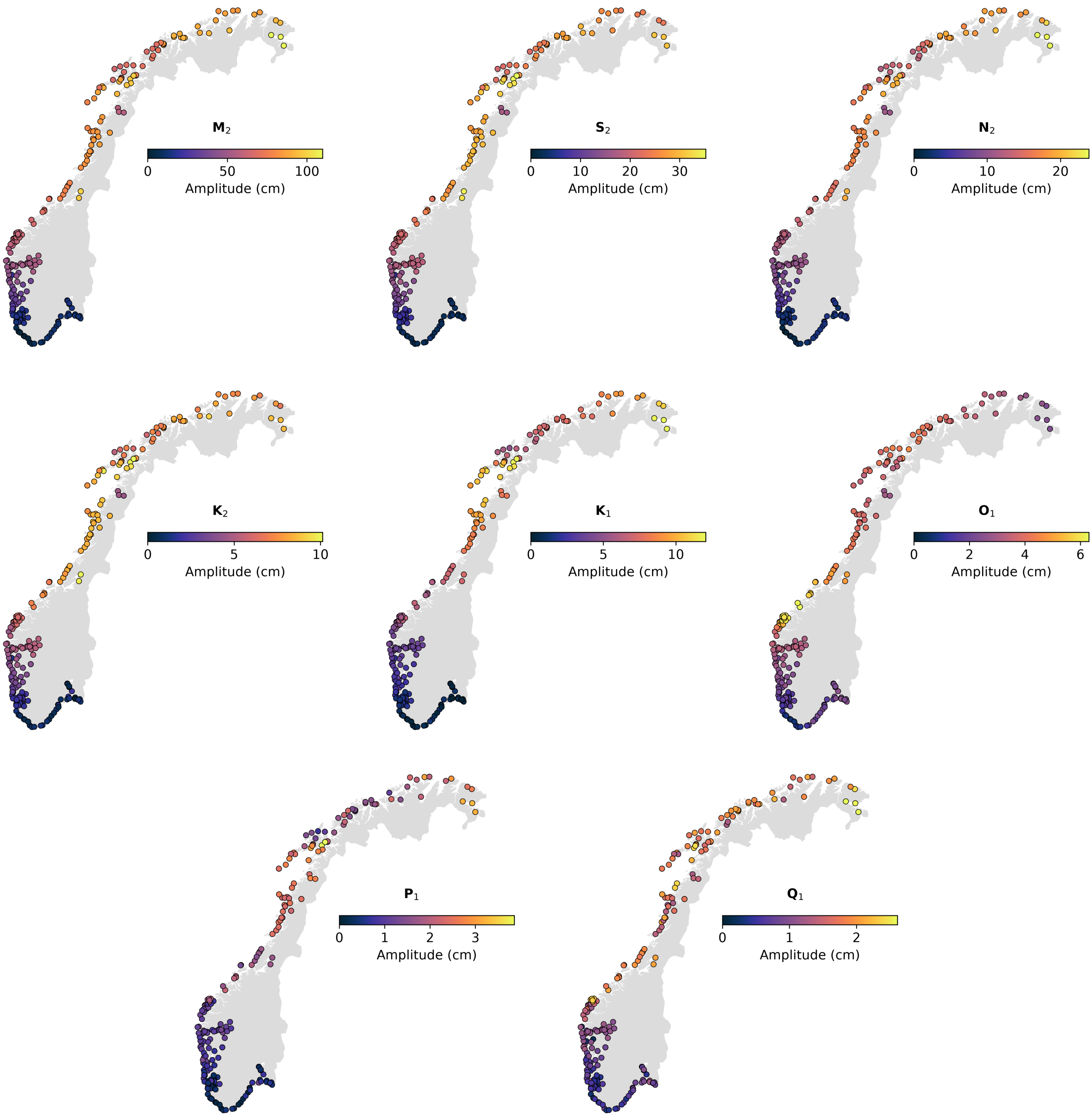


**Figure 3.** Amplitudes of the major eight tidal constituents for all tide gauges. The constituents are presented in order of mean amplitude.

https://doi.org/10.5194/egusphere-2026-5493
Preprint. Discussion started: 16 September 2026


The observational field is therefore characterised by two superimposed scales of variability: a coherent regional tidal regime and complemented local departures from that regime associated with increasingly complex coastal environments. The $M_2$ constituent most clearly exemplifies this behaviour, with the general amplitude pattern being matched by the other tides but at much smaller amplitudes. Local deviations from this general pattern become increasingly evident where the coastline is interrupted by fjords, islands, and narrow passages (e.g. near Skjerstadfjorden and near Trondheim). Several closely situated stations record distinct $M_2$ amplitudes, indicating that the regional tidal signal can be modified over spatial scales much shorter than the distance between conventional long-term tide gauges. Fjord observations further demonstrate that coastal modification is not unidirectional. Landward progression can result in either amplification or attenuation of the tidal amplitude, and some gauge sequences indicate non-monotonic behaviour within individual systems. The amplitude response is therefore dependent on the bathymetry and geometry of each fjord, including variations in depth, cross-sectional area, constrictions, and sills. Detailed attribution of these variations requires analysis at the scale of the individual fjord and cannot be determined from national maps alone. Selected regions with dense observation networks, including Norway's largest fjord system, Sognefjorden, therefore provide natural candidates for higher-resolution investigation.

Phase lags offer a complementary perspective on the Norwegian tidal field by illustrating how the response to astronomical forcing varies spatially along the coastline (Figure 4). Unlike the relatively coherent regions of high and low amplitudes described previously, the phase fields display a more spatially heterogeneous pattern. For the $M_2$ constituent, a systematic progression is observed along the coastline, consistent with the propagation of the semidiurnal tidal wave around the Norwegian margin (Gjevik and Straume, 1989). Other semidiurnal constituents demonstrate similar coastwise organisation, although the magnitude and spatial gradients of phase change differ among them. The modelled amphidromic point is well captured by these observations, a feature missed by the long-term data records (Figure A2). As with amplitude, deviations from the coastwise phase progression become particularly apparent in geometrically complex coastal regions. Local phase differences between neighbouring stations indicate that fjords, narrow passages, and significant bathymetric gradients and transitions can introduce additional temporal variations relative to the broader regional propagation pattern. Skjerstadfjorden is again a key example of this, with the phase lags varying considerably for each tidal constituent.

Collectively, the amplitude and phase observations characterise the Norwegian tidal field as comparatively coherent at regional scales, but increasingly heterogeneous at finer spatial resolutions. The consistent amplitude structure reflects the large-scale tidal regime, while local variations in amplitude and phase highlight the influence of geographically complex features such as fjords, constrictions, and other coastal geometries. This finer-scale structure is effectively captured by the dense tide-gauge network. In contrast, it remains challenging to discern from conventional, sparsely distributed tide-gauge observations alone.

### 3.2 Tidal datums

Tide gauges have been used to produce datums that are used by a variety of scientific disciplines and activities, ranging from ecological functioning (Brand et al., 2023; Beemster et al., 2026) to shipping and navigation (Filmer et al., 2024). In Hart-Davis et al. (2026a), several of these datums were published using GESLA-4 data, including the maximum tidal range and tidal

https://doi.org/10.5194/egusphere-2026-5493
Preprint. Discussion started: 16 September 2026


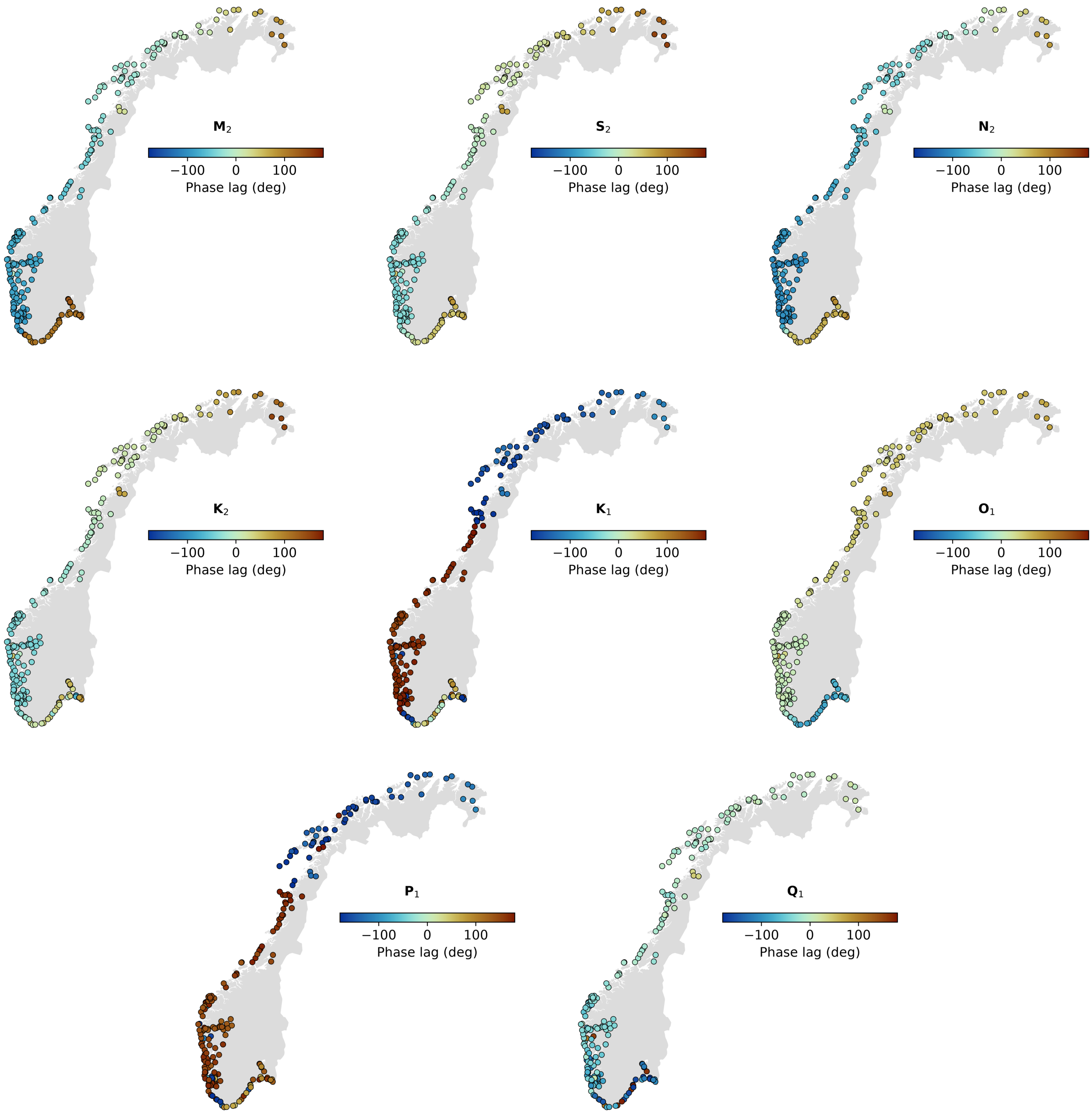


**Figure 4.** Phase lag of the major eight tidal constituents for all tide gauges.

https://doi.org/10.5194/egusphere-2026-5493
Preprint. Discussion started: 16 September 2026


duration. In Figure 5, we provide insights into several tidal datums across the coasts of Norway to supplement these global findings. An important note is that these datums are based on tidal predictions over 20 years; however, in some of these gauges, the record length allows recovery of fewer constituents. The results are still scientifically interesting, but extended data records would clearly improve the accuracy of these data.

The Highest and Lowest Astronomical Tides (HAT and LAT) are key datums that mark the highest and lowest predicted astronomical tides over the 20-year tidal prediction period and are used in navigation and fishing (Williams et al., 2018). From this, we can determine the maximum tidal range as the difference between the two metrics, i.e., HAT minus LAT. What we observe in these three datums (Figure 5a-c) is that the magnitudes of these metrics increase from the southern to the northern coastline. The maximum tidal range reaches 4 metres in northern Norway, with 74% of gauges recording ranges exceeding 1 metre. Across the gauges, a similar increase from south to north is observed with the Mean Higher High Water (MHHW; (Figure 5d), with a median MHHW of 0.65 metres and only 14% of gauges exceeding 1 metre. The MHHW represents the average height of the higher high water level each day over the 20-year period and is a commonly used datum by coastal and oceanographic agencies, e.g., NOAA, as a threshold above which flooding may occur (Miller and Luscher, 2019).

Using this derived threshold as a proxy, in Figure 5e, the mean tidal duration above MHHW was calculated from all the tide gauges. To do so, for each tide gauge, constituents were derived and then used to make a tidal prediction over a 20-year period. Using this tidal prediction, the duration above MHHW is calculated for the entire 20-year period. The results show how long a high-tide stand may last above this threshold, which is important for assessing potential risks to locations, such as tide-influenced compound flooding (Talke, 2025). Along the Norwegian coast, the duration is mostly between 1 and 2 hours, with the southern part of Norway exceeding 3 hours for long stretches of coast. Regarding the latter, this would mean that this coast is more susceptible to compound flooding effects; however, due to the relatively low tidal range in this region (Figure 5c), the risk of tide-influenced coastal flooding is minimal. For the rest of the coast, the one- to two-hour duration produces a relatively small window during which tide-influenced compound flooding can occur. However, this knowledge remains important for coastal mitigation and planning to address such extreme sea-level events.

The final statistic presented is ‘Dodginess’, first introduced in Hart-Davis et al. (2026a), which indicates how much the tidal range varies from one tidal cycle to the next. This is calculated with:

$$Dodginess = 1 - \frac{|A_{K_1} - A_{O_1}| + |A_{M_2} - A_{S_2}|}{A_{K_1} + A_{O_1} + A_{M_2} + A_{S_2}} \quad (1)$$

where A is the respective amplitudes of the subscripted tidal constituents. The idea is that if this value is close to 1, the tide is more ‘dodgy’, i.e., the tidal range varies considerably between tidal cycles. In contrast, towards zero, the tidal range is rather consistent. We employ this method rather than a form-factor approach, which we found to be relatively uniform across the domain, being predominantly semi-diurnal. It should be noted that for Dodginess we utilise all constituents, regardless of whether they satisfy the Rayleigh criteria as discussed earlier. We evaluated the potential impact of errors on the resulting Dodginess estimate (not shown) and found it to be negligible.

In terms of ‘Dodginess’, the coast of Norway is rather consistent in close proximity to 0.5, except for a ‘dodgy’ region along the southwestern coastline. This is the region of the amphidromic point and relatively small tidal variations, where

https://doi.org/10.5194/egusphere-2026-5493
Preprint. Discussion started: 16 September 2026


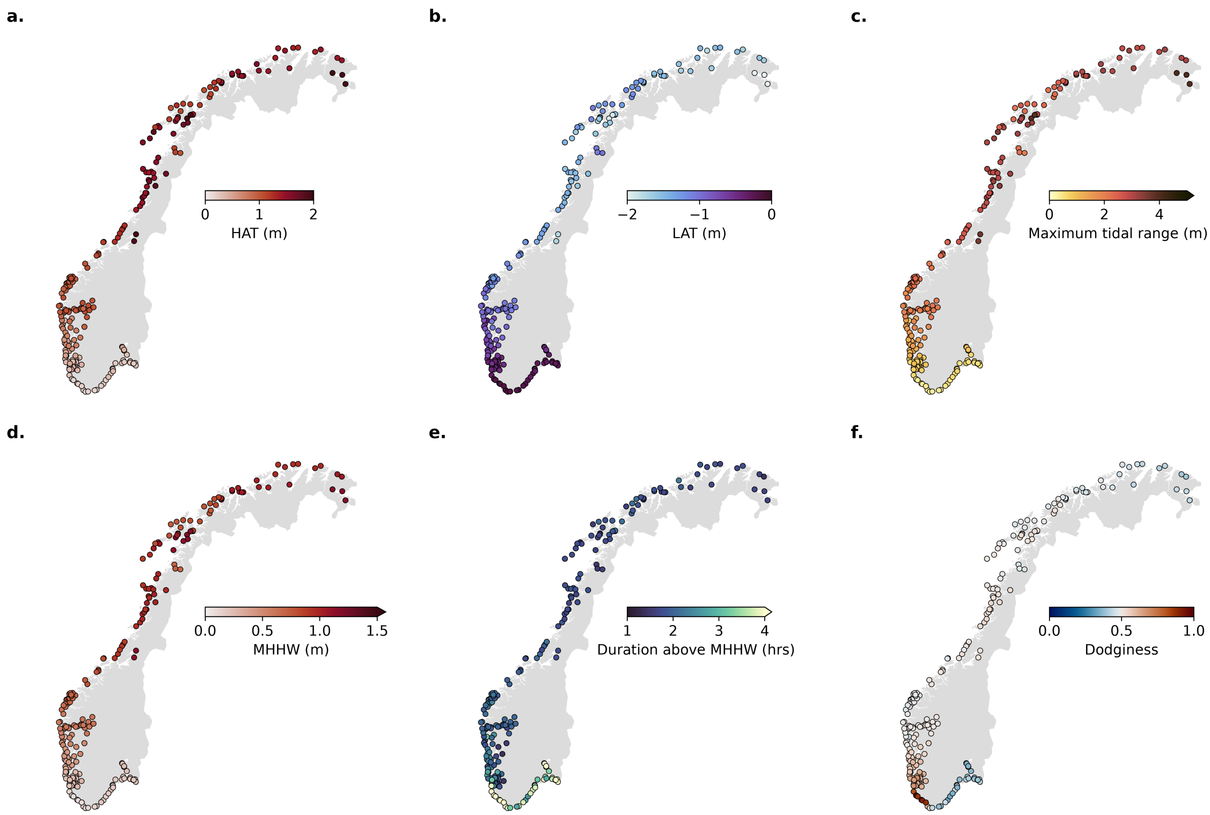


**Figure 5.** Tidal datums extracted from the tide gauge network: a) highest astronomical tide (HAT), b) lowest astronomical tide (LAT), c) maximum tidal range, d) mean higher high water (MHHW), e) mean tidal duration (in hours) above MHHW, and f) Dodginess.

smaller constituents can better compete and cause local variations compared to regions dominated by larger tides, especially the $M_2$ constituent. This would result in greater variability between tidal cycles; however, because the tides in this region (Figure 5c) are rather low, the intercycle variability is itself small. For the remainder of the coastline, values cluster around 0.5, which is characteristic of a conventionally semi-diurnal-dominated regime (Figure 3). In this region, with rather small diurnal contributions, the Dodginess essentially reduces to the relation between $S_2$ and $M_2$, typically yielding a Dodginess of 0.5. This is rather simply illustrated if we assume a ratio of 1:3 for the amplitudes of $S_2$ and $M_2$, which is the approximate relation in this region (more precisely 1:2.96), and treat the diurnals as negligible in Equation 1; the Dodginess equation then reduces to $1 - \frac{2}{4} = 0.5$. This corresponds to the expected fortnightly variability in tidal range, the spring-neap tidal cycle.

### 3.3 Validation of global ocean tide models

A major value of these data is that they provide an independent validation dataset for global modelling. This is particularly valuable in a complex coastal environment such as the Norwegian coast, where numerous islands, inlets, and fjords strongly

https://doi.org/10.5194/egusphere-2026-5493
Preprint. Discussion started: 16 September 2026


influence tidal changes, yet their spatial variability is challenging for model grids to capture accurately. Using the dense network of the 250 gauges, we compare against five state-of-the-art global ocean tide models (Figure 6). Each of these models either directly incorporates conventional nadir satellite altimetry through empirical tidal analysis or does so via data assimilation/inversion methods.

The resulting RSS for each model is shown in Figure 6. Overall, the RSS of EOT26 and FES2022 is the lowest, averaging 2.4 cm, as shown qualitatively in Figure 6 along the coastline. This is largely to be expected, as both of these models have higher spatial resolutions ( 3 km) compared to the other models, which operate at resolutions between 7 km and 18.5 km and have median errors of 3.1 - 3.3 cm. This increased spatial resolution is important in complex regions, such as the Sognefjorden, where these models have significantly lower error than the other models.

For each model, errors increase northward from the southern coast, in agreement with the changes in coastal tidal range (reported in Figure 5c). This biases the interpretation of the RSS somewhat, as the relative differences between observations and models are, in fact, reduced northward along the coast. This relative RSS is calculated as RSS divided by the sum of the amplitudes of the eight major constituents at each location. Throughout the domain, the median percentage difference is 25%, exceeding 50% for most of the southern coastline. For context, the validation of FES2022 with TICON-4 globally results in a median relative difference of 4%, making the median differences in this region significantly higher than the global average. This highlights the complexity of the Norwegian coastline and the placement of these short-duration gauges within the domain.

To quantify this, we classify the tide gauges by their locations to provide insights into how well models perform under varying conditions. This classification uses the GEBCO22 product, places a 10 km-radius grid over each tide gauge location, and then calculates the percentage of land within these grids. We then sort these observations into three categories: ‘low complexity’ being gauges with percentages below the 33rd percentile; ‘medium complexity’ being gauges between the 33rd and 67th percentiles; and ‘high complexity’ being gauges above the 67th percentile. This results in gauges classified as ‘high complexity’ mainly being within fjords, with ‘medium complexity’ gauges found in complex bays, harbors, and larger fjords, while ‘low complexity’ gauges are mainly ocean-facing (see the classifications in Figure 7c).

In Figure 7a, the mean and standard deviation ensemble RMS for each category are shown. As expected, gauges in lower-complexity regions in terms of land coverage have lower RMS values from the models, while higher complexity is associated with increasing errors. This is further illustrated in Figure 7b, where we also estimate the distance of the tide gauges from the open ocean. This is calculated using a Dijkstra algorithm (Dijkstra, 1959; van der Walt et al., 2014) to find the shortest in-water path from the tide gauge to the 200-metre isobath, as defined by GEBCO22. This shows that the further inland the tide gauge, the higher the RMS of the models, and that higher land coverage in the vicinity of the gauge increases error; i.e., tide gauges in more complex locations are harder to model.

A final statistic worth assessing is sinuosity, which serves as a proxy for how twisty or complex a location is. Since we have the derived distance to open water, we can calculate sinuosity by dividing the Dijkstra-derived path length to open water by the direct distance to the same open water location. A value of 1 in this case would mean the gauge is directly aligned with the open water, while higher values would indicate that the path to the gauge becomes more complex. Qualitatively, Figure 7c suggests that increasing sinuosity is associated with an increase in ensemble RMS with moderate correlation between the

https://doi.org/10.5194/egusphere-2026-5493
Preprint. Discussion started: 16 September 2026


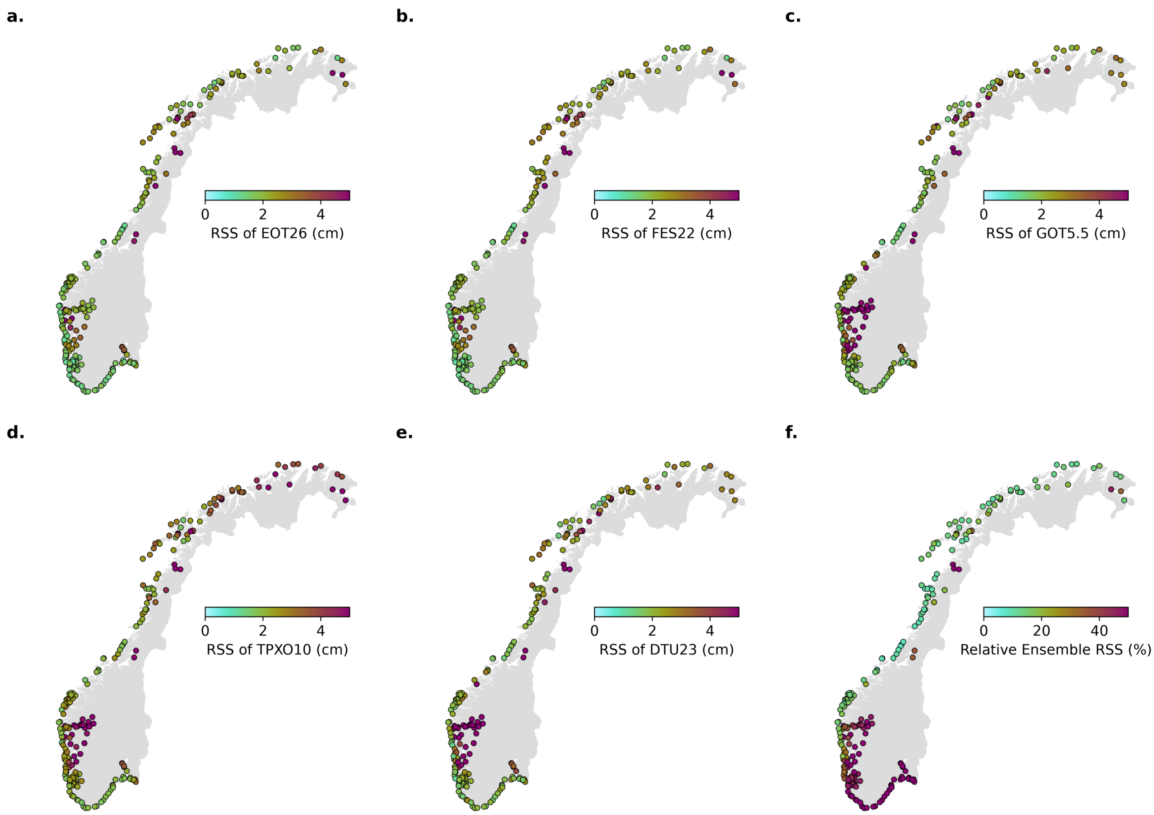


**Figure 6.** RSS of the major eight tidal constituents from EOT26 (a), FES2022 (b), GOT5.5 (c), TPXO10 (d), DTU23 (e), and a relative ensemble of all these models (f).

two statistics ($\rho = 0.5$). This suggests that fjord geometry does influence error, but, as seen in Figure 7b, gauge positioning and the complexity of the surrounding coastline are also crucial contributors to model error. Because model error in absolute terms scales with the size of the tide, we first tested whether coastal complexity is itself correlated with tidal amplitude along the Norwegian coast. Ensemble model error correlates moderately with both tidal amplitude (Spearman $\rho = 0.48$) and coastal complexity ($\rho = 0.35$), while the two properties are themselves only weakly correlated ($\rho = -0.21, p < 0.001$), indicating that they act as largely independent controls on model performance. This is seen in Figure 7a: model error along this coastline is therefore governed largely by coastal geometry, independent of the regional tidal regime.

To test whether this reflects the model's spatial resolution, we derived the slope of model RMS against land fraction for each model, with tidal amplitude fitted alongside to separate the two effects. This slope represents the rate at which a model's error grows as the coastline becomes more enclosed, measured in centimetres per unit land area. We determine an overall ensemble slope (and standard errors) of the model RMS of $2.65 \pm 0.28$ cm per unit land fraction, which, when analysed individually, is $1.41 \pm 0.20$ and $1.30 \pm 0.20$ for EOT26 and FES2022, the two highest resolution models, compared with $2.69 \pm 0.41$, 2.76

https://doi.org/10.5194/egusphere-2026-5493
Preprint. Discussion started: 16 September 2026


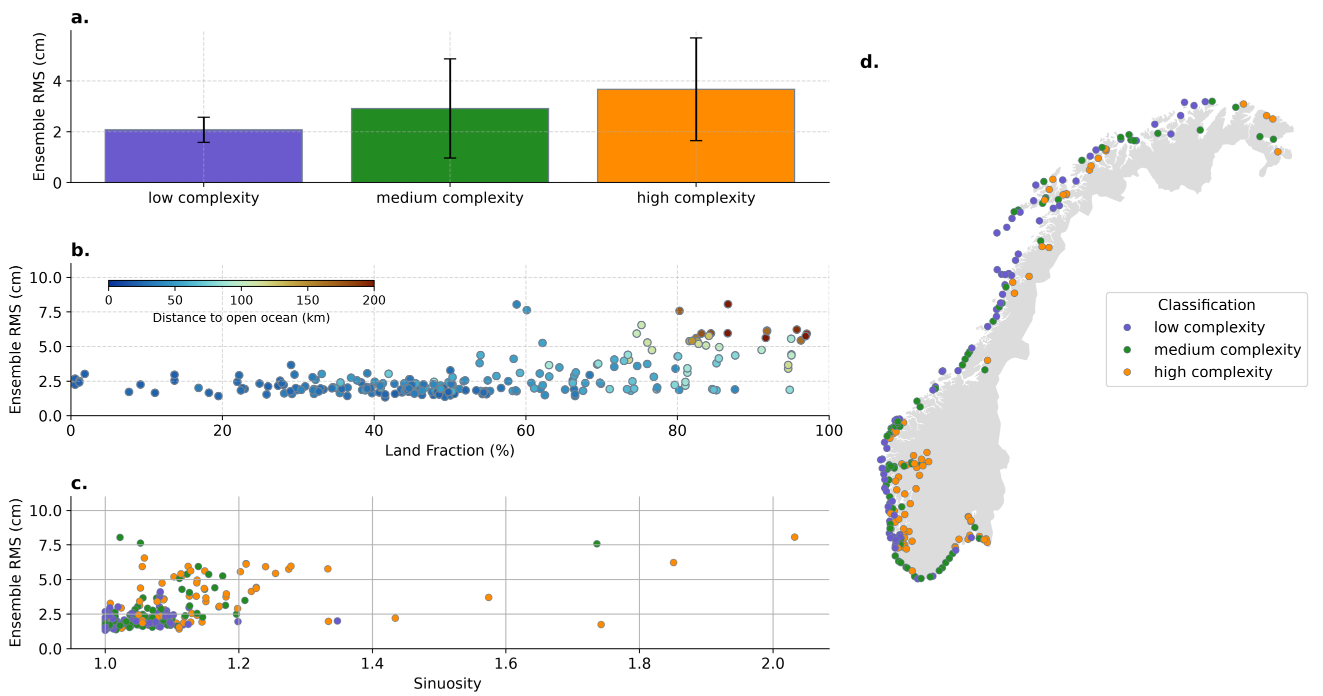


**Figure 7.** Classification of the ensemble model errors for all the tide gauges. a) Is the mean error, with standard deviations) within each classified level of land complexity, b) the error as a function of percentage land fraction surrounding the gauge, and c) the error as a function of sinuosity. d) Presents an atlas of the domain classification results.

$\pm$ 0.28 and 3.22 $\pm$ 0.49 for GOT5.5, TPXO10 and DTU23 respectively, for the coarser resolution models. This suggests that along the coast of Norway, high-resolution tide models are essential for accurately capturing the spatial variability of tides. This presents an exciting opportunity for novel measurement techniques, such as the SWOT satellite, which can observe tides with a spatial resolution as fine as 50 metres (Hart-Davis et al., 2024).

## 4 Conclusion

Historically, tide gauges have been the most important method of observing ocean tides, allowing us to understand local dynamics and develop local forecasts. The challenge, though, has always been their coverage and availability. Along complex coastlines, such as the Norwegian coast, gauge coverage plays a vital role in capturing fine-scale variations caused by islands, inlets, and fjords. The dense network of 250 tide gauges deployed by Kartverket and presented in this manuscript, therefore, provides a highly significant increase in the spatial coverage of observations that, in turn, allows for the analyses and interpretation of tidal dynamics at an unprecedented scale.

https://doi.org/10.5194/egusphere-2026-5493
Preprint. Discussion started: 16 September 2026


We observe from the individual tidal constituents that the tides of Norway increase from south to north, with the southern side having rather tiny tidal amplitudes. This is largely due to the amphidromic point on the southwestern coast. This results in the datums, particularly the tidal range, increasing nearly linearly along the coast, with the maximum tidal range observed at the most northeastern tide-gauge location, Nesseby, in the Barents Sea. However, we also observe that within complex fjords and inlets, fine-scale variations in tides can be observed that would not be captured from permanent gauge stations.

The comparisons with global models driven by conventional nadir altimetry clearly highlight a particular challenge: reliable modelling of the tides around Norway, given the complexity of the coastline. In this context, advanced satellite observation methods, such as the wide-swath observations from the Surface Water and Ocean Topography (SWOT) satellite, have the potential to inform and improve model predictions in these regions. In Hart-Davis et al. (2024), SWOT was shown to observe tides at greatly improved spatial scales in previously challenging regions. It is therefore expected that the use of SWOT-based data across the complex coastal and fjord regions of Norway will enable novel research into tidal dynamics.

*Data availability.* The tidal constituents of the major eight tides with their respective amplitudes and phase lags, and associated errors are available at SEANOE: https://doi.org/10.17882/119454 (Hart-Davis et al., 2026b). The raw gauge data is available from Kartverket upon request. TICON-4 is available at: https://doi.org/10.17882/109129 (Hart-Davis et al., 2025). The GEBCO dataset can be found at: https://doi.org/10.5285/4f68d5c7-45eb-f999-e063-7086abc036fa and GESLA-4 at: https://gesla787883612.wordpress.com/downloads/.

*Author contributions.* M.G.H.D. conceptualised and produced the results of the manuscript. M.G.H.D and B.E.T. interpreted and discussed the results and produced the first draft of the manuscript. T.T. provided the input data for this manuscript. All authors wrote, reviewed, and approved the final draft of this manuscript.

*Competing interests.* The contact author has declared that none of the authors has any competing interests.

*Acknowledgements.* The authors would like to thank colleagues at the Norwegian Mapping Authority, Kartverket, for making these data available for this study. This work was supported by the Norwegian Space Agency (NoSA) through the project “Novel Insights into Tides and Coastal Sea Level Variability Along the Norwegian Land-Ocean Continuum: SWOT Capabilities” (Contract No. 74CO2611).

https://doi.org/10.5194/egusphere-2026-5493
Preprint. Discussion started: 16 September 2026


# Appendix

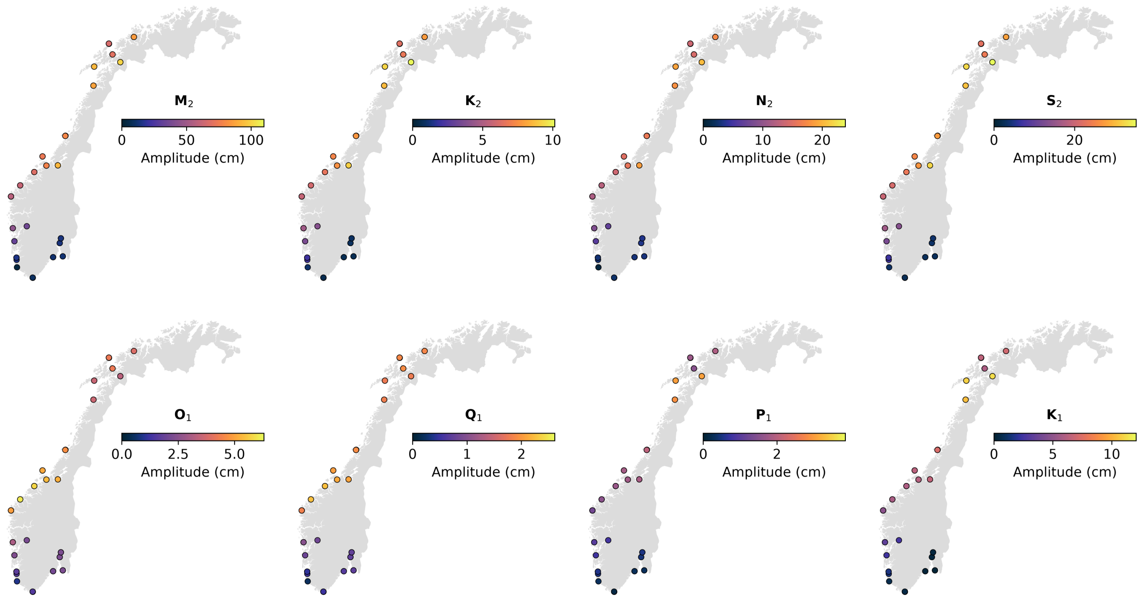


**Figure A1.** Amplitude of the major eight tidal constituents taken from the TICON-4 dataset.

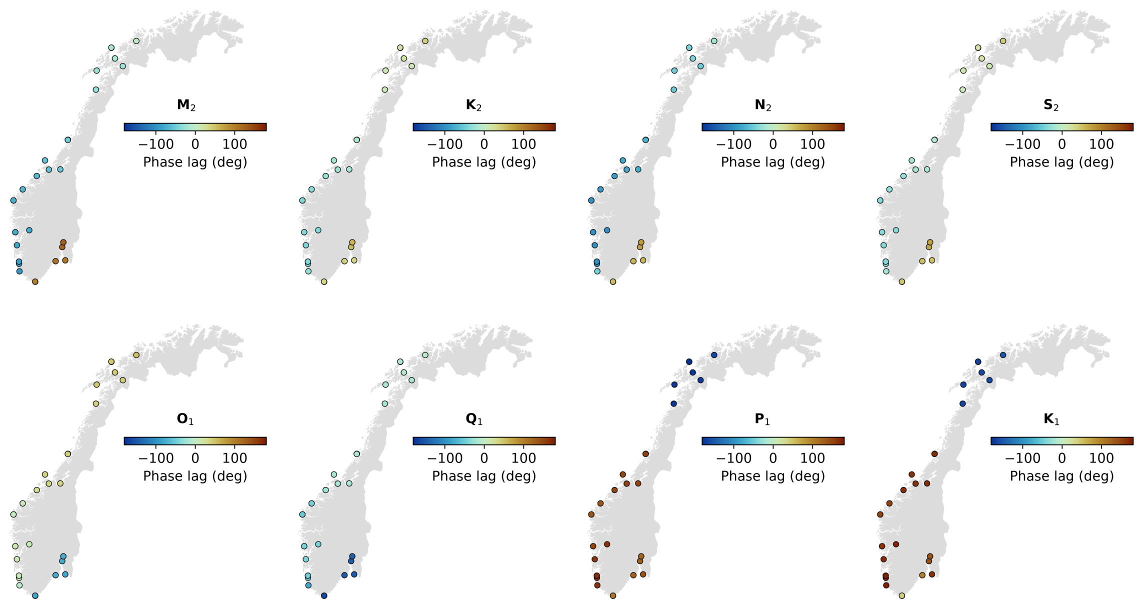


**Figure A2.** Phase lag of the major eight tidal constituents taken from the TICON-4 dataset.

https://doi.org/10.5194/egusphere-2026-5493
Preprint. Discussion started: 16 September 2026


## References

Andersen, O. B., Rose, S. K., and Hart-Davis, M. G.: Polar Ocean Tides – Revisited Using Cryosat-2, Remote Sensing, 15, 4479, https://doi.org/10.3390/rs15184479, 2023.

Beemster, J. G. W., Talke, S. A., Van Maren, D. S., Giloy, N., Wünsche, A., Zhang, W., Grasso, F., and Hoitink, A. J. F.: Human footprint on estuarine tidal hydrodynamics, Nature Geoscience, 19, 620–629, https://doi.org/10.1038/s41561-026-01969-4, 2026.

Brand, M. W., Diefenderfer, H. L., O'Connor, J. E., Borde, A. B., Jay, D. A., Al-Bahadily, A., McKeon, M. A., and Talke, S. A.: Impacts of a Cascadia Subduction Zone earthquake on water levels and wetlands of the lower Columbia River and Estuary, Geophysical Research Letters, 50, e2023GL103 017, https://doi.org/10.1029/2023GL103017, 2023.

Breili, K., Simpson, M. J. R., Klokkervold, E., and Roaldsdotter Ravndal, O.: High-accuracy coastal flood mapping for Norway using lidar data, Natural Hazards and Earth System Sciences, 20, 673–694, https://doi.org/10.5194/nhess-20-673-2020, 2020.

Cartwright, D. E., Edden, A. C., Spencer, R., and Vassie, J. M.: The tides of the northeast Atlantic Ocean, Philosophical Transactions of the Royal Society of London. Series A, 298, 87–139, https://doi.org/10.1098/rsta.1980.0241, 1980.

Codiga, D. L.: Unified tidal analysis and prediction using the UTide MATLAB functions, Tech. Rep. URI/GSO Technical Report 2011-01, Graduate School of Oceanography, University of Rhode Island, Narragansett, Rhode Island, https://doi.org/10.13140/RG.2.1.3761.2008, 2011.

Dijkstra, E. W.: A note on two problems in connexion with graphs, Numerische Mathematik, 1, 269–271, https://doi.org/10.1007/BF01386390, 1959.

Egbert, G. D. and Erofeeva, S. Y.: Efficient inverse modeling of barotropic ocean tides, Journal of Atmospheric and Oceanic Technology, 19, 183–204, https://doi.org/10.1175/1520-0426(2002)019<0183:EIMOBO>2.0.CO;2, 2002.

Filmer, M. S., Johnston, P. J., Jayaswal, Z., Taylor, A., Chittleborough, J., Claessens, S. J., Seifi, F., Kuhn, M., McCubbine, J., and Entel, M.: Connecting land and sea vertical datums: a data evaluation for developing Australia's AUSHYDROID model, Marine Geodesy, 47, 183–213, https://doi.org/10.1080/01490419.2024.2305898, 2024.

Filmer, M. S., Woodworth, P. L., Williams, S. D. P., and Claessens, S. J.: Analysis of the uncertainties in tidal constants obtained from short tide gauge records and their value for tidal studies, Continental Shelf Research, 295, 105 565, https://doi.org/10.1016/j.csr.2025.105565, 2025.

Gjevik, B. and Straume, T.: Model simulations of the $M_2$ and the $K_1$ tide in the Nordic Seas and the Arctic Ocean, Tellus A, 41, 73–96, https://doi.org/10.3402/tellusa.v41i1.11822, 1989.

Gjevik, B., Nøst, E., and Straume, T.: Model simulations of the tides in the Barents Sea, Journal of Geophysical Research: Oceans, 99, 3337–3350, https://doi.org/10.1029/93JC02743, 1994.

Gjevik, B., Moe, H., and Ommundsen, A.: Sources of the Maelstrom, Nature, 388, 837–838, https://doi.org/10.1038/42159, 1997.

Hart-Davis, M., Dettmering, D., and Seitz, F.: TICON-4: TIdal CONstants based on GESLA-4 sea-level records, https://doi.org/10.17882/109129, 2025.

Hart-Davis, M. G., Piccioni, G., Dettmering, D., Schwatke, C., Passaro, M., and Seitz, F.: EOT20: a global ocean tide model from multi-mission satellite altimetry, Earth System Science Data, 13, 3869–3884, https://doi.org/https://doi.org/10.5194/essd-13-3869-2021, 2021.

Hart-Davis, M. G., Andersen, O. B., Ray, R. D., Zaron, E. D., Schwatke, C., Arildsen, R. L., Dettmering, D., and Nielsen, K.: Tides in complex coastal regions: early case studies from wide-swath SWOT measurements, Geophysical Research Letters, 51, e2024GL109 983, https://doi.org/10.1029/2024GL109983, 2024.

https://doi.org/10.5194/egusphere-2026-5493
Preprint. Discussion started: 16 September 2026


Hart-Davis, M. G., Sulzbach, R., Talke, S. A., Haigh, I. D., Marcos, M., Woodworth, P. L., Ray, R. D., Andersen, O. B., Lyard, F., Fouchet, E., Dettmering, D., Thomas, M., and Seitz, F.: Tide of the Time: global tidal characteristics observed from in-situ measurements, Ocean Science, 22, 1681–1709, https://doi.org/10.5194/os-22-1681-2026, 2026a.

Hart-Davis, M. G., Torunski, B., Bonaduce, A., Taskjelle, T., and Johannessen, J. A.: Tidal constituents of Norway (ToN) from temporary gauges, https://doi.org/10.17882/119454, 2026b.

Hjelmervik, K. B., Kristensen, N. M., Staalstrøm, A., and Røed, L. P.: A simple approach to adjust tidal forcing in fjord models, Ocean Dynamics, 67, 949–958, https://doi.org/10.1007/s10236-017-1067-y, 2017.

Jänicke, L., Ebener, A., Dangendorf, S., Arns, A., Schindelegger, M., Niehüser, S., Haigh, I. D., Woodworth, P., and Jensen, J.: Assessment of tidal range changes in the North Sea from 1958 to 2014, Journal of Geophysical Research: Oceans, 126, e2020JC016 456, https://doi.org/10.1029/2020JC016456, 2021.

Kubiak, K.: Kystvakten – Norwegian Coast Guard, Studia Maritima, 32, 207–230, https://doi.org/10.18276/sm.2019.32-09, 2019.

Lyard, F. H., Allain, D. J., Cancet, M., Carrère, L., and Picot, N.: FES2014 global ocean tide atlas: design and performance, Ocean Science, 17, 615–649, https://doi.org/10.5194/os-17-615-2021, 2021.

Lynge, B. K., Berntsen, J., and Gjevik, B.: Numerical studies of dispersion due to tidal flow through Moskstraumen, northern Norway, Ocean Dynamics, 60, 907–920, https://doi.org/10.1007/s10236-010-0309-z, 2010.

Miller, A. and Luscher, A.: NOAA's National Water Level Observation Network (NWLON), Journal of Operational Oceanography, 12, S57–S66, https://doi.org/10.1080/1755876X.2018.1523301, 2019.

Piccioni, G., Dettmering, D., Bosch, W., and Seitz, F.: TICON: TIdal CONstants based on GESLA sea-level records from globally located tide gauges, Geoscience Data Journal, 6, 97–104, https://doi.org/10.1002/gdj3.72, 2019.

Pugh, D. T., Woodworth, P. L., and Bos, M. S.: Lunar tides in Loch Ness, Scotland, Journal of Geophysical Research: Oceans, 116, C11 040, https://doi.org/10.1029/2011JC007411, 2011.

Ray, R. D.: Documentation for Goddard Ocean Tide Solution GOT5: Global Tides from Multi-mission Satellite Altimetry, NASA Tech. Memo. 20250002085, Goddard Space Flight Center, Greenbelt MD, https://ntrs.nasa.gov/api/citations/20250002085/downloads/GOT5-TechMemo.pdf, 2025.

Sætra, Ø., Halsne, T., Carrasco, A., Breivik, Ø., Pedersen, T., and Christensen, K. H.: Intense interactions between ocean waves and currents observed in the Lofoten Maelstrom, Journal of Physical Oceanography, 51, 3461–3476, https://doi.org/10.1175/JPO-D-20-0290.1, 2021.

Stammer, D., Ray, R. D., Andersen, O. B., Arbic, B. K., Bosch, W., Carrère, L., Cheng, Y., Chinn, D. S., Dushaw, B. D., Egbert, G. D., Erofeeva, S. Y., Fok, H. S., Green, J. A. M., Griffiths, S., King, M. A., Lapin, V., Lemoine, F. G., Luthcke, S. B., Lyard, F., Morison, J., Müller, M., Padman, L., Richman, J. G., Shriver, J. F., Shum, C. K., Taguchi, E., and Yi, Y.: Accuracy assessment of global barotropic ocean tide models, Reviews of Geophysics, 52, 243–282, https://doi.org/10.1002/2014RG000450, 2014.

Talke, S. A.: How tidal properties influence the future duration of coastal flooding, npj Natural Hazards, 2, 36, https://doi.org/10.1038/s44304-025-00086-3, 2025.

van der Walt, S., Schönberger, J. L., Nunez-Iglesias, J., Boulogne, F., Warner, J. D., Yager, N., Gouillart, E., and Yu, T.: scikit-image: image processing in Python, PeerJ, 2, e453, https://doi.org/10.7717/peerj.453, 2014.

Wessel, P., Luis, J. F., Uieda, L., Scharroo, R., Wobbe, F., Smith, W. H. F., and Tian, D.: The Generic Mapping Tools Version 6, Geochemistry, Geophysics, Geosystems, 20, 5556–5564, https://doi.org/10.1029/2019GC008515, 2019.

Williams, J., Irazoqui Apecechea, M., Saulter, A., and Horsburgh, K. J.: Radiational tides: their double-counting in storm surge forecasts and contribution to the Highest Astronomical Tide, Ocean Science, 14, 1057–1068, https://doi.org/10.5194/os-14-1057-2018, 2018.